Direct Calibration of a Laser Ablation System in the Projective Voltage Space

Adrian Schneider[1,2], Simon Pezold[1], Kyung-won Baek[1], Dilyan Marinov[2], and Philippe C. Cattin[1,2]

[1] Department of Biomedical Engineering, University of Basel, Switzerland
[2] Advanced Osteotomy Tools AG, Basel, Switzerland

Abstract. Laser ablation is a widely adopted technique in many contemporary medical applications. However, it is new to use a laser to cut bone and perform general osteotomy surgical tasks with it. In this paper, we propose to apply the *direct linear transformation* algorithm to calibrate and integrate a laser deflecting tilting mirror into the affine transformation chain of a sophisticated surgical navigation system, involving next generation robots and optical tracking. Experiments were performed on synthetic input and real data. The evaluation showed a *target registration error* of 0.3 mm ± 0.2 mm in a working distance of 150 mm.

Keywords: Robotics, Navigation, Laser, Mirror, DLT.

1 Introduction

Laser ablation is a tissue cutting technique that is widely adopted in ophthalmology and dentistry. Although such a *contact-free* cutting method would also be beneficial when cutting bones, i.e. in osteotomy, only little research has been invested in this area so far. One major reason for this was the lack of a compact laser source able to efficiently cut bone without carbonizing it.

With the proposed laser osteotome, see Fig. 1, we try to bridge this gap. To guarantee a high cutting precision, the laser source is directly mounted on a robot's end effector and is optically tracked using a stereo optical tracking device. A reflective mirror mounted on a 2-axes tilting mirror stage was introduced to deflect the laser beam. This tilting mirror permits quickly changing the direction of the laser beam. Large displacements are covered by the robot arm, whereas the small changes in the target location are handled by the tilting mirror. The question remains on how to align a voltage controlled mirror with the coordinate systems (CS) of the optical tracker, patient, and robot.

In this paper, we present a robust method to calibrate the tilting mirror and integrate it into the affine transformation chain. The essence of our approach is to apply a projective camera model to the given situation. In reference to Fig. 2, the camera center C corresponds to the mirror's laser deflecting spot D, from where light rays are received or emitted in a conical manner. In the case of an

N. Navab et al. (Eds.): MICCAI 2015, Part I, LNCS 9349, pp. 274–281, 2015.
DOI: 10.1007/978-3-319-24553-9_34

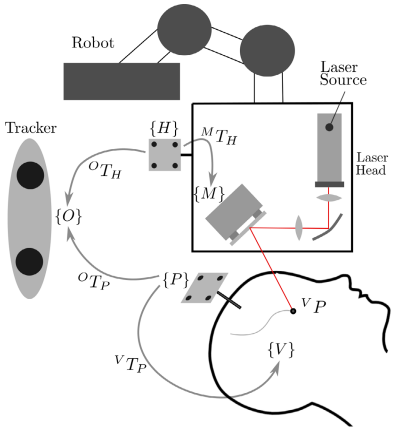

Fig. 1. Navigated laser system. Arrows denote affine transformations.

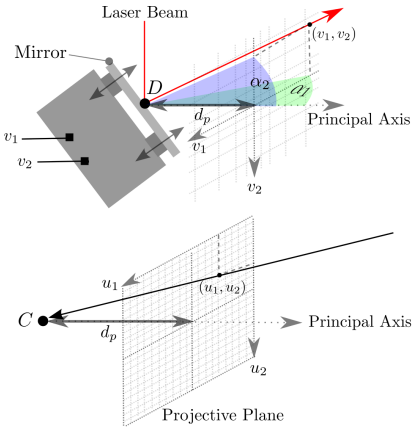

Fig. 2. Analogy of a laser tilting mirror (top) and a camera (below).

actual digital camera, the projective plane is an equidistant grid of photosensors u_1, u_2, whereas the mirror operates in a *virtual* voltage space v_1, v_2.

In the field of computer vision, well established camera calibration methods exist. In 1971, Abdel-Aziz and Karara introduced the *Direct Linear Transformation* (DLT) [1], which was a commonly used but rudimentary calibration technique. The main difference to contemporary calibration algorithms is that DLT does not consider nonlinear lens distortion effects, such as radial or tangential distortion. However, this is not required in the case of reflective optics as only mirrors and no lenses are involved. An interesting property of the DLT is that the extrinsic and intrinsic mirror parameters can be determined simultaneously.

In robotics, comparable work has been done on laser rangefinders, which perform depth measurements by triangulation of a moving laser beam and a camera [5]. Unfortunately, they focus only on extrinsic parameters and take the laser's steering properties (intrinsic) as given. The same pattern can be observed in many other applications. Often, the optical path and the mechanics, such as the steering mirror, are known very accurately. It makes sense to use this information and lock as many degrees of freedom as possible. In our system, the intrinsic parameters of the tilting mirror are known as well. But for two reasons we cannot use them: First, the optical setup of our prototype laser head is changing frequently. Second and more importantly, the regulatory authorities require the system to be calibrated on a regular basis when used in clinical practice, which certainly involves the determination of the mirror's overall properties.

Interesting related publications can be found in the field of catadioptric systems. From there we learned that it is common to apply a pinhole model to describe a moving mirror with a fixed center of reflection. A comparable situation is described in [4]. However, the setup there involves a hyperbolic mirror and a camera, which has to be calibrated with a non-linear approach. Our situation is comparably simple and we show that applying the DLT is appropriate.

2 Methods

2.1 Tilting Mirror Calibration with the DLT

As an input, the DLT algorithm requires several 2D–3D point correspondences. Using the pinhole camera model (Fig. 2), the projection of the i-th point from 3D spatial coordinates ${}^{H}X_i = [x, y, z, 1]_i^T$ to 2D pixel coordinates $u_i = [u_1, u_2, 1]_i^T$ on the projection plane is generally given by

$$\kappa u_i = \tilde{K} \cdot {}^{M}T_H \cdot {}^{H}X_i \Leftrightarrow \kappa \begin{bmatrix} u_1 \\ u_2 \\ 1 \end{bmatrix}_i = \begin{bmatrix} \tilde{f}_1 & 0 & \tilde{c}_1 \\ 0 & \tilde{f}_2 & \tilde{c}_2 \\ 0 & 0 & 1 \end{bmatrix} \cdot \begin{bmatrix} r_{11} & r_{12} & r_{13} & t_1 \\ r_{21} & r_{22} & r_{23} & t_2 \\ r_{31} & r_{32} & r_{33} & t_3 \end{bmatrix} \cdot \begin{bmatrix} x \\ y \\ z \\ 1 \end{bmatrix}_i , \quad (1)$$

with the intrinsic parameter matrix $\tilde{K}$ and the affine transformation ${}^{M}T_H$, where $\tilde{K}$ holds the focal distances $\tilde{f}_j$ and the principal point coordinates $\tilde{c}_j$ $(j = 1, 2)$, ${}^{M}T_H$ consists of a rotation part $r_{11}, \ldots, r_{33}$ and a translation part t_1, t_2, t_3, and κ is a normalization constant. In our model, ${}^{M}T_H$ represents the rigid transformation of the mirror's CS $\{M\}$ with respect to the optical marker's CS $\{H\}$ (Fig. 1). The corresponding spatial coordinate ${}^{H}X_i$ is expressed in the $\{H\}$ CS and denotes the 3D point where the laser beam impacts.

Choosing the distance from the projective center to the projective plane $d_p = 1$, u_j $(j = 1, 2)$ can be rewritten as $u_j = \tan(\alpha_j)$, where α_j denotes the angles of the two axes in which the deflection mirror is tilted. The angles are unknown, but they are linear to the known applied voltages v_j, enabling us to rewrite them as $\alpha_j = a_j v_j + b_j$ with the linearity parameters a_j, b_j. Putting these reformulations together, we can rewrite the projection as

$$\kappa \begin{bmatrix} \tan(a_1 v_1 + b_1) \\ \tan(a_2 v_2 + b_2) \\ 1 \end{bmatrix}_i = \tilde{K} \cdot {}^{M}T_H \cdot {}^{H}X_i. \quad (2)$$

The small-angle approximation enables us to simplify $\tan(\alpha_j) \approx \alpha_j$ $(\alpha_j < 10°)$, thus $\tan(a_j v_j + b_j) \approx a_j v_j + b_j$, which we use to simplify the projection as

$$\kappa \hat{C} \begin{bmatrix} v_1 \\ v_2 \\ 1 \end{bmatrix}_i \approx \tilde{K} \cdot {}^{M}T_H \cdot {}^{H}X_i \quad \text{with} \quad \hat{C} = \begin{bmatrix} a_1 & 0 & b_1 \\ 0 & a_2 & b_2 \\ 0 & 0 & 1 \end{bmatrix} . \quad (3)$$

Combining $\hat{C}$ and $\tilde{K}$ leads to the final approximative projection from spatial coordinates to voltage space:

$$\kappa v_i = \kappa \begin{bmatrix} v_1 \\ v_2 \\ 1 \end{bmatrix}_i \approx K \cdot {}^{M}T_H \cdot {}^{H}X_i \quad \text{with} \quad K = \hat{C}^{-1}\tilde{K} = \begin{bmatrix} f_1 & 0 & c_1 \\ 0 & f_2 & c_2 \\ 0 & 0 & 1 \end{bmatrix} , \quad (4)$$

where K holds the new intrinsic parameters f_j $(= \frac{\tilde{f}_j}{a_j})$ and c_j $(= \frac{\tilde{c}_j}{a_j} - \frac{b_j}{a_j})$.

We would like to point out two important aspects of the final model. First, it is feasible for small tilting angles only. This holds in our case, as our mirror is operated in a range of $\pm 6°$, resulting in a relative approximation error of 0.4%. Second, the actual angle–voltage relation need not be known, in fact: K and ${}^{M}T_{H}$ are calculated solely from correspondences between voltage pairs v_i and 3D points ${}^{H}X_i$, both of which are known. Showing the relationship between v_i, K and $u_i, \tilde{K}$ was only necessary to establish the model.

The vector v_i is proportional to the vector $[K \cdot {}^{M}T_{H} \cdot {}^{H}X_i]$, see Eq. (4). As a consequence, their crossproduct ($\times$) is 0. Applying the DLT, we find K and ${}^{M}T_{H}$ by solving for their product $P = K \cdot {}^{M}T_{H}$, which leads to

$$v_i \times \left(P \cdot {}^{H}X_i\right) = 0 \quad \Leftrightarrow \quad \begin{bmatrix} v_1 \\ v_2 \\ 1 \end{bmatrix}_i \times \left(\begin{bmatrix} p_{11}\ p_{12}\ p_{13}\ p_{14} \\ p_{21}\ p_{22}\ p_{23}\ p_{24} \\ p_{31}\ p_{32}\ p_{33}\ p_{34} \end{bmatrix} \cdot \begin{bmatrix} x \\ y \\ z \\ 1 \end{bmatrix}_i \right) = 0, \tag{5}$$

with $p_{11} \ldots p_{34}$ as unknowns and $[v_1, v_2]_i^T$, $[x, y, z]_i^T$ given by the point correspondences. This can be converted into a linear system of equations

$$A \cdot \begin{bmatrix} p_{11} \\ \vdots \\ p_{34} \end{bmatrix} = 0 \quad \text{with} \quad A = \begin{bmatrix} 0 & 0 & 0 & 0 & -x_0 & -y_0 & -z_0 & 1 & v_{2_0}x_0 & v_{2_0}y_0 & v_{2_0}z_0 & v_{2_0} \\ x_0 & y_0 & z_0 & 1 & 0 & 0 & 0 & 0 & -v_{1_0}x_0 & -v_{1_0}y_0 & -v_{1_0}z_0 & -v_{1_0} \\ \cdots & & & & & & & & & & & \\ 0 & 0 & 0 & 0 & -x_i & -y_i & -z_i & 1 & v_{2_i}x_i & v_{2_i}y_i & v_{2_i}z_i & v_{2_i} \\ x_i & y_i & z_i & 1 & 0 & 0 & 0 & 0 & -v_{1_i}x_i & -v_{1_i}y_i & -v_{1_i}z_i & -v_{1_i} \\ \cdots & & & & & & & & & & & \\ 0 & 0 & 0 & 0 & -x_N & -y_N & -z_N & 1 & v_{2_N}x_N & v_{2_N}y_N & v_{2_N}z_N & v_{2_N} \\ x_N & y_N & z_N & 1 & 0 & 0 & 0 & 0 & -v_{1_N}x_N & -v_{1_N}y_N & -v_{1_N}z_N & -v_{1_N} \end{bmatrix}. \tag{6}$$

Each correspondence results in three equations, one of which is redundant due to linear dependence. Thus, a number of $N \geq 6$ correspondences is required to solve for the 12 unknowns. The resulting product P can then be decomposed into K and ${}^{M}T_{H}$ as described in [3].

Input Data Normalization: The algorithm described above is the basic DLT. To enhance the numerical stability, we first transform the 2D–3D point correspondences in order to reach certain spatial properties. In [3], this can be found as *Normalized DLT*. In the presence of measurement noise, it is highly recommended to normalize the input data.

2.2 Calibration Errors

Due to the small-angle approximation and measurement noise, the computed solution K, ${}^{M}T_{H}$ will not map the given N input 2D–3D correspondences perfectly. Several error measures can be applied to quantify the quality of the calibration procedure. The *algebraic error* is the residual of the underlying least squares problem in Eq. (6). The *backprojection error* E is a geometric error quantity in the voltage plane. With the computed calibration result, the acquired 3D points ${}^{H}X_i$ are virtually projected as v_i' and compared with corresponding voltage pairs v_i by computing their Euclidean distances, as

$$E_i = \left\| v_i - v_i' \right\| \quad \text{with} \quad v_i' \propto K \cdot {}^{M}T_{H} \cdot {}^{H}X_i \quad \text{for} \quad i = 1, \ldots, N. \tag{7}$$

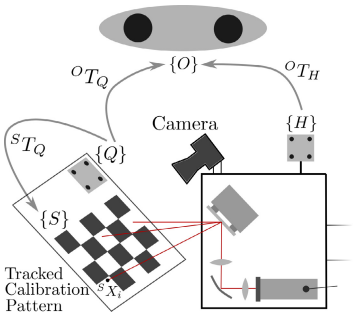

Fig. 3. Acquiring correspondences with a tracked calibration pattern.

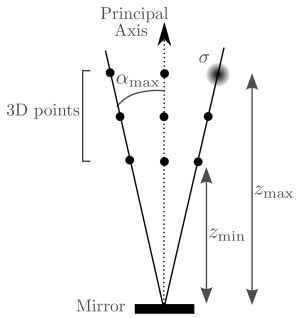

Fig. 4. Synthetic input data generation for the calibration.

The most important error measure for surgeons is the deviation from the planned location on the target site, i.e. on the patient herself and in millimetre, the so called *target registration error* (TRE). An error in the voltage plane E_i can be extrapolated with the distance between tilting mirror and target d_i, which is easy to determine after transforming the 3D points into the mirror CS. The TRE T_i is then computed for all N point correspondences as

$$T_i = d_i \left\| K^{-1} \cdot [E_i, 0, 0]^T \right\| \quad \text{with} \quad d_i = \left\| {}^{M}T_H \cdot {}^{H}X_i \right\| \quad \text{for} \quad i = 1, \ldots, N. \tag{8}$$

2.3 Acquiring 2D–3D Correspondences

The accuracy of the mirror calibration depends strongly on the quality of its input data. Figure 3 illustrates our acquisition setup. The robot is driven into an appropriate position. Then $N_v \geq 1$ predefined voltage pairs v_i $(i = 1, \ldots, N_v)$ are applied to the tilting mirror. Their laser impact on a chessboard is recorded with a camera, and the standard blob-detector of *OpenCV* is used to recover their pixel positions, which can be easily transformed into the given chessboard CS ${}^{S}X_i$. It is important to notice that recovering ${}^{S}X_i$ with the camera is an independent process. Neither the relative position of the camera to the tilting mirror nor the rest of the system matters. However, a focused image preferably orthogonal to the chessboard enhances the accuracy of acquired positions.

In order to transform the laser position from the chessboard CS $\{S\}$ into the laser head CS $\{H\}$, first one has to resolve the transformation from the chessboard to its tracked marker ${}^{S}T_Q$. A common method based on fitting two 3D point sets [2] was applied for that purpose. The final transformation is

$${}^{H}X_i = \left({}^{O}T_H\right)^{-1} \cdot {}^{O}T_Q \cdot \left({}^{S}T_Q\right)^{-1} \cdot {}^{S}X_i, \tag{9}$$

where ${}^{O}T_Q$ and ${}^{O}T_H$ are given by the optical tracking system.

These steps are repeated from N_p different robot positions. Therefore, the total amount of collected 2D–3D correspondences is $N = N_v N_p$. A simple robot trajectory is orthogonal to the chessboard surface.

2.4 Integration of the Tilting Mirror

Using the notation introduced in Fig. 1, the transformations ${}^{O}T_H$ and ${}^{O}T_P$ are given by the tracking system. The 3D–3D registration ${}^{V}T_P$ from the patient marker to the operation planning data (CT, MR) can be performed with the method described in [2]. Given a cutting position ${}^{V}P$ on the patient, the two voltages (v_1, v_2) for the mirror can be computed by

$$\left[v_1, v_2, 1\right]^T \propto K \cdot {}^{M}T_H \cdot \left({}^{O}T_H\right)^{-1} \cdot {}^{O}T_P \cdot \left({}^{V}T_P\right)^{-1} \cdot {}^{V}P, \tag{10}$$

which finally forms the complete transformation chain.

3 Experiments and Results

In this section, the performance of the described calibration approach is examined in detail based on synthetic and real input data. These experiments were performed by applying the normalized DLT approach.

Error Analyses with Synthetic Input Data: In these experiments, synthetic data was produced to analyze the presented method in terms of error behavior. As illustrated in Fig. 4, the calibration data generation can be configured by the four parameters $\alpha_{\max}$ (maximum angle for both mirror axes), $z_{\min}$ and $z_{\max}$ (distance in principal direction between the mirror and the 3D points), N_v (number of different voltage pairs applied in each robot position), N_p (number of different robot positions), and σ (standard deviation of zero-mean Gaussian noise applied to the 3D points). The point correspondences are generated in a deterministic way. For our simulated tilting mirror, v_1, v_2 are chosen to be equal to α_1, α_2 (1°/voltage). Based on a given $\alpha_{\max}$, an equidistant voltage array of size N_v is generated, where values of both axes α_1, α_2 are in the range of $-\alpha_{\max} \leq \alpha_{1,2} \leq \alpha_{\max}$. These are the 2D points. Their corresponding 3D coordinates are generated by applying this voltage array to the mirror and projecting to N_p different orthogonal planes with distance z_p, so that $z_0 = z_{\min}, \ldots, z_{N_p} = z_{\max}$. As already mentioned, this leads to a total number of $N = N_v N_p$ point correspondences. To simulate the presence of noise, zero-mean Gaussian noise σ is added in all three dimensions to each 3D coordinate.

Maximum Deflection Angle Influence: Since the proposed method is based on the small-angle approximation, calibrations with increasing maximum deflection angle were performed. In particular, synthetic data sets with varying $\alpha_{\max} = 2°, \ldots, 8°$ were generated, whereas the other parameters were kept constant at $z_{\min}$ =140 mm and $z_{\max}$ =160 mm, $\sigma = 0$, $N_v = 25$, and $N_p = 5$. Of each of these data sets, the mirror calibration was computed and the TRE T_i was determined and presented as a box plot, where the central mark is the median, the edges of the box are the 25th and 75th percentiles and the whiskers extend to the minimum and maximum errors. Figure 5 shows the results.

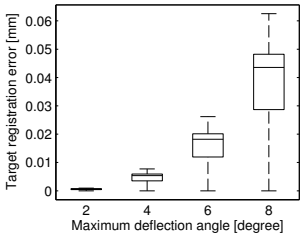

Fig. 5. TRE with increasing maximum mirror angle $\alpha_{\max}$.

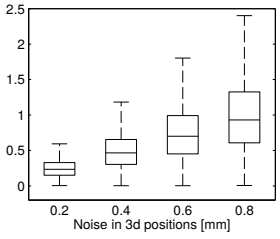

Fig. 6. TRE with increasing Gaussian noise σ.

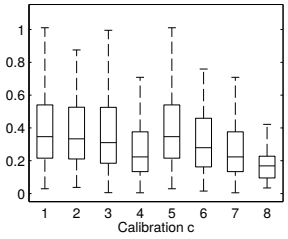

Fig. 7. TRE for real acquired correspondences.

Impact of Noise: In this experiment, calibrations with increasing Gaussian noise $\sigma = 0.2\,\text{mm}, \ldots, 0.8\,\text{mm}$ were made. Other parameters remained constant at $\alpha_{\max} = 6°$, $z_{\min} = 140\,\text{mm}$, $z_{\max} = 160\,\text{mm}$, $N_v = 25$, and $N_p = 5$. For each noise level, $N_c = 100$ calibrations were made. Figure 6 shows the resulting TRE.

Results: One can clearly see that the tangent approximation for small angles is unproblematic. In our system, the maximum deflection angle $\alpha_{\max}$ is 6°, which corresponds to a maximum TRE of about 30 µm. Measurement noise, however, is an issue. The reported accuracy of our used tracking system is 0.25 mm. Based on the simulation, this corresponds to a TRE of about 0.5 mm.

Calibration with Real Data: In this experiment, the proposed calibration method was tested within the actual laser ablation system. As a tilting mirror, the OIM5001 (Optics In Motion) was used. The used optical tracking system was the CamBar B2 (AXIOS 3D Services) and the robot was the iiwa (KUKA Laboratories). The distance z between the chessboard and the tilting mirror was around 150 mm. The maximum deflection angle $\alpha_{\max}$ was about 6°. However, since the extrinsic and intrinsic mirror properties ${}^{M}T_{H}$, K are unknown at this time, the exact values of z and α can be determined only afterwards.

In the following, $N_c = 8$ independent tilting mirror calibrations were done. For each calibration c, $N_p = 5$ different robot positions along the chessboard normal were used. In each position, $N_v = 25$ voltage pairs were applied. Therefore, the maximum number of 2D–3D correspondences for each calibration c was $N = 125$. But due the regularly failure of the visual blob-detection within black chessboard fields, N showed to easily drop to 80.

Results: The results of the 8 calibrations can be seen in Fig. 7. The average TRE is 0.3 mm, with a standard deviation of 0.2 mm. The maximum error is 1.0 mm. The average distance z between the mirror and all involved correspondences was 141 mm and the average $\alpha_{\max}$ was 6.8°. When comparing the measured error with the results of noisy synthetic input data, this meets the expected error when using an optical tracking device with a spatial accuracy of 0.25 mm.

Fig. 8. The laser system performing a navigated cut on a sheep head.

Fig. 9. Enlarged view of the cutting region. The bright spot is the laser.

4 Conclusion

We showed that a voltage controlled tilting mirror can be accurately calibrated by using the pinhole camera model and the *direct linear transformation* approach to solve it. With a *target registration error* of $0.3\,\text{mm} \pm 0.2\,\text{mm}$ at a working distance of 150 mm, our laser ablation system not only exceeds general osteotomy requirements, but also opens up new surgical possibilities in terms of cutting shapes. Although a maximum cutting error of 1.0 mm is tolerable, it does not meet our own demands. Currently we are designing non-planar optical markers to increase the tracking accuracy. Preliminary results are promising.

To conclude, we would like to give the reader an impression of the presented laser system in action. Figures 8 and 9 show a navigated cut on a sheep skull.

References

1. Abdel-Aziz, Y., Karara, H.: Direct Linear Transformation from Comparator Coordinates Into Object Space Coordinates in Close-range Photogrammetry (1971)
2. Arun, K.S., Huang, T.S., Blostein, S.D.: Least-squares fitting of two 3-D point sets. IEEE Trans. on Pattern Analysis and Machine Intelligence (5), 698–700 (1987)
3. Hartley, R., Zisserman, A.: Multiple view geometry in computer vision. Cambridge Univ Press (2010)
4. Orghidan, R., Salvi, J., Mouaddib, E.M.: Calibration of a structured light-based stereo catadioptric sensor. In: Conference on Computer Vision and Pattern Recognition Workshop, CVPRW 2003, vol. 7, p. 70. IEEE (2003)
5. Zhang, Q., Pless, R.: Extrinsic calibration of a camera and laser range finder. In: Proceedings of the 2004 IEEE/RSJ International Conference on Intelligent Robots and Systems (IROS 2004), vol. 3, pp. 2301–2306. IEEE (2004)